



PERGAMON

Deep-Sea Research II 49 (2002) 4791–4806

DEEP-SEA RESEARCH
PART II

www.elsevier.com/locate/dsr2

Long-term temperature trends in the deep waters of the Weddell Sea

Robin Robertson^{a,*}, Martin Visbeck^a, Arnold L. Gordon^a, E. Fahrbach^b

^a Lamont-Doherty Earth Observatory, Columbia University, 10964 Palisades, NY, USA

^b Alfred-Wegener-Institut, Postfach 12 0161, D-27515 Bremerhaven, Germany

Accepted 16 March 2002

Abstract

Warming of the deep water in the Weddell Sea has important implications for Antarctic bottom water formation, melting of pack ice, and the regional ocean–atmosphere heat transfer. In order to evaluate warming trends in the Weddell Sea, a historical data set encompassing CTD and bottle data from 1912 to 2000 was analyzed for temporal trends in the deep water masses: warm deep water (WDW) and Weddell Sea deep water (WSDW).

The coldest WDW temperatures were primarily associated with the Weddell Polynya of the mid-1970s. Subsequent warming occurred at a rate of $\sim 0.012 \pm 0.007^\circ\text{C yr}^{-1}$ from the 1970s to 1990s. This warming was comparable to the global, average surface water warming observed by Levitus et al. (Science 287 (2000) 2225), to the warming of the WSBW in the central Weddell Sea observed by Fahrbach et al. (Filchner–Ronne Ice Shelf Program, Report No. 12, Alfred-Wegener-Institut, Bremerhaven, Germany, 1998a, p. 24), and to the surface ice temperature warming from 1970 to 1998 in the Weddell Sea observed by Comiso (J. Climate 13 (2000) 1674). The warming was not compensated by an increase in salinity, and thus the WDW became less dense. The location of the warmest temperature was displaced towards the surface by ~ 200 m from the 1970s to the 1990s. Although the average WSDW potential temperatures between 1500 and 3500 m were warmer in the 1990s than in the 1970s, high variability in the data prevented identification of a well-defined temporal trend.

© 2002 Elsevier Science Ltd. All rights reserved.

1. Introduction

The Weddell Sea (Fig. 1) is one of the primary source regions of Antarctic bottom water (AABW) (Deacon, 1937). WSDW formed in the Weddell

Sea through mixing of warm deep water (WDW) or modified warm deep water (MWDW) with shelf or ice shelf waters is transformed through further mixing in the Scotia Sea into AABW. Changes in the deep water masses in the Weddell Sea will eventually impact AABW production and thus the deep ventilation and global thermohaline circulation. The local ocean–atmosphere heat exchange may be affected by changes in the deep water masses, since heat loss from the deep waters to the surface mixed layer melts the surface ice and

*Corresponding author. Tel.: + (845) 365-8527; fax: + (845) 365-8157.

E-mail addresses: rroberts@ldeo.columbia.edu (R. Robertson), visbeck@ldeo.columbia.edu (M. Visbeck), agordon@ldeo.columbia.edu (A.L. Gordon), efahrbach@awi-bremerhaven.de (E. Fahrbach).

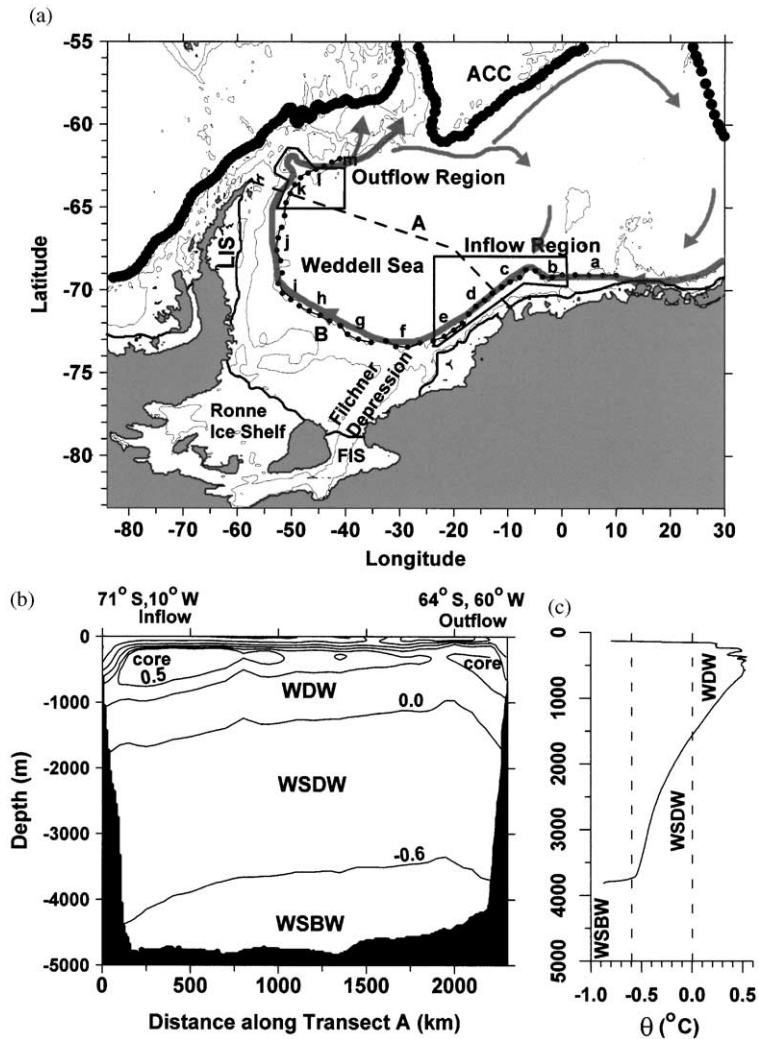


Fig. 1. (a) The bathymetry for the Weddell Sea with contours shown at 500 and 3000 m. The locations of transects A (SR4) and B are indicated by dashed and dotted lines, respectively, and labeled with the respective characters. The segments of transect B are indicated and labeled a–m. The location and direction of the core of the Weddell Gyre current are indicated by gray lines and arrows. The southern extent of the Antarctic circumpolar current is shown by a series of large black dots and labeled ACC (coordinates were kindly provided by A. Orsi (personal communication)). The edges of the Larsen, Ronne, Filchner, Brunt, and Riiser–Larsen Ice Shelves are indicated by solid lines and the ice shelves are labeled (LIS for the Larsen Ice Shelf and FIS for the Filchner Ice Shelf). The regions used to determine the inflow and outflow characteristics are indicated by boxes and labeled accordingly. (b) Typical hydrography along transect A from east to west. The potential temperature, θ , is shown contoured at 0.5°C, 0.35°C, 0.0°C, -0.6°C and -1.3°C. The deep water masses, including WDW, WSDW, and WSBW, are identified. The surface waters are not labeled. The warm core of WDW near the inflow and outflow regions with θ values greater than 0.5°C and 0.35°C, respectively, are denoted “core”. (c) A sample potential temperature, θ , profile with depth for the Weddell Sea (at 66°S 48°W). The portions of the profile, which are WDW, WSDW and WSBW, are identified.

influences the heat transfer from the ocean to the atmosphere (Gordon and Huber, 1990; McPhee and Martinson, 1994; McPhee et al.,

1996; Gordon, 1998; Muench et al., 2002). Consequently, the long-term variability of the deep waters in the Weddell Sea has important

implications for the regional ocean–atmosphere heat transport, the global thermohaline circulation, and the ventilation of the deep ocean. Several programs were developed in order to investigate deep-water production and ventilation and their variation, including deep ocean ventilation through Antarctic intermediate layers (DOVE-TAIL) (Muench and Hellmer, 2002), the Southern Ocean component of Consortium for ocean’s role in climate (CORC) (Visbeck et al., 2001), and the set of repeated transects across the Weddell Sea collected by Alfred-Wegener-Institut (Schröder and Fahrbach, 1999; Fahrbach et al., 1994a, 2001).

The world’s surface oceans, defined by Levitus as within 300 m of the surface, have warmed from the mid-1950s to the mid-1990s by an average of 0.31°C , $\sim 0.007^{\circ}\text{C yr}^{-1}$ (Levitus et al., 2000). For the Weddell Sea, satellite measurements indicate that the surface ice temperatures warmed at rates up to $0.01\text{--}0.02^{\circ}\text{C yr}^{-1}$ from 1979 to 1998 (Comiso, 2000). Less is known about warming of the deep waters, although Gordon (1982) found the deep water in the Weddell Sea to be cooling from the mid-1950s to 1980, with a sharp decrease from 1973 to 1977, and Fahrbach et al. (1998a) found the Weddell Sea bottom water (WSBW) to be warming by $\sim 0.01^{\circ}\text{C yr}^{-1}$ from 1989 to 1995. Here, we aim to evaluate changes in the temperature of the deep water masses in the Weddell Sea using historical conductivity/temperature/depth (CTD) and bottle data collected west of 10°E and spanning the last 30 years.

2. Historical hydrographic data set

The available CTD and bottle data for the Weddell Sea from the National Oceanographic Data Center (NODC) data set (Conkright et al., 1998) and assorted sources at Lamont–Doherty Earth Observatory (LDEO) (Table 1) were assembled. The LDEO data included observations collected as part of the WOCE, CORC (1999 and 2000), DOVETAIL (1997), and Ice Station Weddell (1992) programs, along with various other cruises listed in Table 1. To this set was added data from the continental slope in the region north of

the Filchner–Ronne Ice Shelf, which were collected as part of the Ronne Polynya Experiment (Ropex) (1998) (Nicholls et al., 1998; Woodgate et al., 1998); data from several cruises of the British Antarctic Survey (see Table 1) (Barber and Crane, 1995); and data from the Alfred-Wegener-Institut (Fahrbach et al., 1994a, 2001). The temperature, T , conductivity, C , and pressure, P , from these CTD profiles were converted to potential temperature, θ , salinity, S , and depth, D using the UNESCO routines (Fofonoff and Millard, 1983).

Some editing of the data was required, primarily due to errors in salinity. Profiles with constant S or θ for all depths of the profile were flagged as unrealistic and removed from the data set (~ 125 profiles). The remaining profiles were visually examined both in $\theta - S$ space and as $\theta - Z$ and $S - Z$ profiles to remove obvious outliers. After editing, 2956 profiles remained, ranging in time from 1912 to 2000. The temporal and spatial distributions of these profiles are shown in Fig. 2. The data were quite sparse before 1970 (Fig. 2). No effort was made to remove the seasonal cycle, which was believed to be smaller than the changes reported here (J. Toole, personal communication). Since most of the data were collected during the austral summer, little aliasing was expected. In order to keep the austral summer months grouped together, the year was defined as starting in October and running through September.

The uncertainty for the data varied for each cruise, but generally decreased for the more recent data. As a general guideline, the uncertainties for the data as described in the literature for the respective cruises are $\pm 0.003^{\circ}\text{C}$ for θ and ± 0.002 psu for S from the 1990s, $\pm 0.003^{\circ}\text{C}$ for θ and ± 0.003 psu for S from the 1980s, $\pm 0.006^{\circ}\text{C}$ for θ and ± 0.005 psu for S from the 1970s, and $\pm 0.02^{\circ}\text{C}$ for θ and ± 0.01 psu for S from the 1960s. Data prior to 1960 have uncertainties equivalent to or greater than those of the 1960s. Some data have higher uncertainties than those typical for the decade. For example, uncertainties for a cruise from 1987 to 1988 were estimated at $\pm 0.01^{\circ}\text{C}$ for θ and ± 0.01 psu for S (Gouretski and Danilov, 1993).

Table 1
List of research cruises included in the historical data set

Data set	Research vessel	Cruise/experiment	Year
NODC	Various	Various	Various—1912–1993
LDEO	<i>James Clark Ross</i>	WOCE A23	1995
	<i>N.P. Palmer</i>	AnzFlux	1994
	<i>Ice Station Weddell</i>	Ice Station Weddell	1992
	<i>Akademic Federov</i>	Ice Station Weddell	1992
	<i>NB Palmer</i>	Ice Station Weddell	1992
	<i>Polarstern</i>	WOCE A12	1992
	<i>San Bernadino</i>	—	1992
	<i>Pacific Dawn</i>	—	1988
	<i>Gen. AM Patch</i>	—	1988
	<i>Glacier</i>	—	1976, 1986
	<i>Melville</i>	AMERIEZ	1981, 1983, 1986
	<i>Knorr</i>	AJAX II	1984
	<i>Mikhail Somov</i>	—	1981
	<i>Atlantis II</i>	—	1980
	<i>Islas Orcadas</i>	—	1976, 1977, 1978
DOVETAIL	<i>NB Palmer</i>	DOVETAIL	1997
CORC-1999	<i>LM Gould</i>	CORC	1999
CORC-2000	<i>LM Gould</i>	CORC	2000
Alfred-Wegener-Institut	<i>Polarstern</i>	AntV	1986–1987
	<i>Polarstern</i>	AntVII	1989
	<i>Polarstern</i>	WWGS/AntVIII	1989
	<i>Meteor</i>	WOCE A9	1990
	<i>Polarstern</i>	AntIX	1990–1991
	<i>Polarstern</i>	AntX	1992–1993
	<i>Polarstern</i>	AntXI	1994
	<i>Polarstern</i>	AntXII	1994–1995
	<i>Polarstern</i>	AntXIII	1996
	<i>Polarstern</i>	AntXV	1998
	<i>Polarstern</i>	AntXVI	1999
		(WOCE SR2, SR4)	
Ropex	<i>James Clark Ross</i>	Ropex	1998
British Antarctic Survey	<i>James Clark Ross</i>	—	1992
	<i>John Biscoe</i>	—	1989–1990
	<i>Discovery</i>	—	1988
	<i>John Biscoe</i>	—	1987

3. Water mass definitions and the general circulation

3.1. Water mass definitions

In the Weddell Sea (Fig. 1a), three primary deep water masses exist: WDW, WSDW, and WSBW (Fig. 1b). Throughout this study, the primary water masses are defined by ranges in the potential temperature, θ ($^{\circ}\text{C}$), and salinity, S (psu), as given in Table 2. The basic hydrography across the

Weddell Sea can be seen in Fig. 1b, which shows the smoothed temperature along transect A (World Ocean Circulation Experiment (WOCE) line SR4) (dashed line in Fig. 1a). Since transect A passes through both the inflow and outflow regions of the Weddell Gyre (Fig. 1a), it shows the warmer core of inflowing WDW in the eastern Weddell Sea with potential temperatures greater than 0.5°C .

WSDW is formed through the mixing of WDW or MWDW with either shelf waters or WSBW.

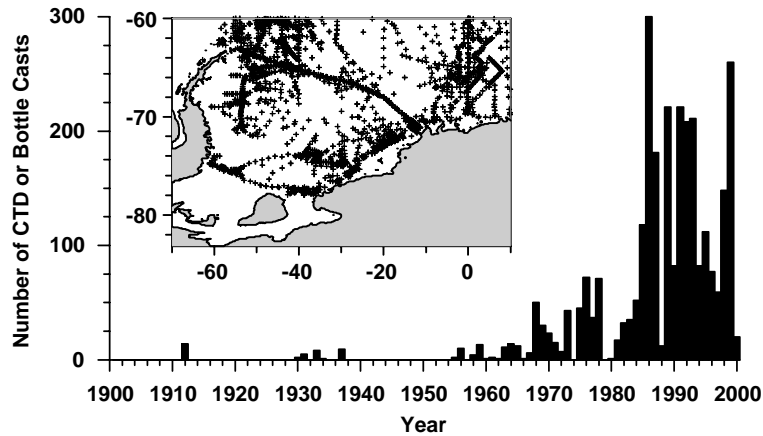


Fig. 2. The distribution of the CTD and bottle data profiles used in the study with time, with the inset showing the locations of the CTD and bottle data profiles as crosses.

Table 2

Potential temperature and salinity ranges for Weddell Sea water masses, adapted from Meredith et al. (2000) and Weppernig et al. (1996) following definitions by Carmack and Foster (1977)

	Water mass	Potential temperature range (°C)	Salinity range (psu)
Surface waters	Surface mixed layer (defined by location in the water column, not potential temperature and salinity)	-1.88 ^a to 1.0	33.0–34.5
Shelf waters	Winter water (WW)	-1.88 ^a to -1.7	34.30–34.44
	Low-salinity shelf water (LSSW)	-1.88 ^a to -1.7	34.3–34.4
	High-salinity shelf water (HSSW)	-1.88 ^a to -1.7	34.56–34.84
Transitional waters	Ice shelf water (ISW)	< -1.9	34.2–34.7
	Modified warm deep water (MWDW)	-0.7 to -1.7	34.4–34.6
Deep waters	Warm deep water (WDW)	0.0 to 1.0	34.6–34.75
	Weddell Sea deep water (WSDW)	-0.6 ^b	34.62–34.68
		-0.7 ^c to 0.0	
		-0.8 ^d	
	Weddell Sea bottom water (WSBW)	-0.6 ^b	34.62–34.68
		-1.3 to -0.7 ^c	
		-0.8 ^d	

^a -1.88 or surface freezing temperature for the salinity present.
^b Definition used in this investigation.
^c Definition used by Meredith et al. (2000) and Weppernig et al. (1996).
^d Definition used by Carmack and Foster (1977).

MWDW refers to WDW, which has mixed with surface waters and is cooler than WDW (Table 2). Unfortunately, no distinct division exists between the WDW and WSDW. As seen in a sample profile for the Weddell Sea collected near 64.25°S,

48.25°W, potential temperature decreases gradually from ~0.4°C to ~-0.6°C (Fig. 1c). Here, the most common upper boundary for the WSDW, the 0.0°C isotherm, was adopted (Carmack and Foster, 1977; Weppernig et al., 1996; Meredith

et al., 2000). Near the bottom of the potential temperature profile (Fig. 1c), a strong temperature gradient exists, starting between -0.6°C and -0.8°C and marking the transition zone between WSDW and WSBW. Different investigators have defined the lower potential-temperature boundary for the WSDW as either -0.6°C , -0.7°C , or -0.8°C (Table 2). Here, we adopt the warmer value (-0.6°C), which is more appropriate for the deeper water depths of the utilized data and assures that all cold contributions are counted as WSBW.

3.2. General circulation

The major feature of the circulation in the Weddell Sea is the clockwise flow of the Weddell Gyre (Fig. 1a). Circumpolar Deep Water from the Antarctic Circumpolar Current (series of large dots in Fig. 1a) enters the Weddell Sea at $\sim 30^{\circ}\text{E}$ and is incorporated into the Weddell Gyre becoming WDW (Deacon, 1979; Orsi et al., 1993; Gordon and Huber, 1995). The WDW transits the gyre, cooling as it progresses, primarily through mixing with cooler water types (Gordon et al., 1998; Schröder and Fahrbach, 1999).

During transit, the WDW mixes with shelf waters, forming WSDW and/or WSBW. Additionally, WSDW and WSBW formed over the continental shelf and slope flow down the continental slope and enter the deep basin along the transect, particularly west of the Filchner depression. Due to the density and depth of the WSBW, it is unable to pass over the Endurance or America–Antarctic Ridges (~ 3000 – 3500 m water depth) and is confined to the basin. The WSDW, however, flows at a shallower depth (Fig. 1b) and is able to pass over the ridges and exit the basin. The WSDW exits the Weddell Sea, primarily through the Scotia Sea, where it is then transformed by further mixing into AABW and flows into the global deep ocean (Locarnini et al., 1993; Whitworth et al., 1994). Gordon (1998) and Fahrbach et al. (1998b) give comprehensive descriptions of the hydrography and circulation in the western and eastern portions of the Weddell Sea, respectively.

3.3. Spatial structure of the thermal stratification along the Weddell Gyre

Although the data set encompassed most of the Weddell Sea (Fig. 2), this study focused on the deep waters flowing around the Weddell Gyre. The best temporal coverage occurred in two regions, an inflow and an outflow region (boxed areas in Fig. 1a). They were selected to evaluate temporal trends and variability. The inflow region in the southeastern Weddell Sea was $\sim 30^{\circ}$ west of the region where the circumpolar deep water enters the Weddell Gyre becoming WDW (Orsi et al., 1993, 1999). We also diagnosed the mean water-mass properties along a transect (B), which connected the two regions, roughly following the 3000-m isobath (Fig. 1). The outflow region covers the area just upstream from where WSDW exits the Weddell Gyre (Gordon, 1998). Both the inflow and outflow regions were considered only at water depths greater than 1000 m in order to avoid contamination by shelf processes. The travel time between the inflow and outflow regions has been estimated to be ~ 2 – 4 years, using mean speeds of ~ 0.04 – 0.08 m s^{-1} and following Fahrbach et al. (1994a, 2001).

Transect B was broken into thirteen 220-km-long segments, each of which was divided into four 55-km sub-segments. The center locations for each sub-segment are indicated in Fig. 1a by dots and the segments are labeled sequentially from a to m. Only data from within 110 km of the center points of the sub-segments were used, and the data were attributed only to the closest sub-segment. To minimize coastal influences, the locations were constrained to water depths between 2500 and 3500 m or well below the limiting depth chosen for the inflow and outflow regions. In order to reduce the temporal variability, only data from 1990–1995 were used.

The predominant structure of the WDW was lower maximum θ values further along the gyre. Using the maximum θ value above 0.0°C , θ_{MAX} , to characterize the WDW, the average θ_{MAX} for the sub-segments decreased by $\sim 1.1 \times 10^{-4}^{\circ}\text{C km}^{-1}$ along transect B (Fig. 3a).

The wide range of θ_{MAX} values within the sub-segments (Fig. 3a) illustrates a primary difficulty in

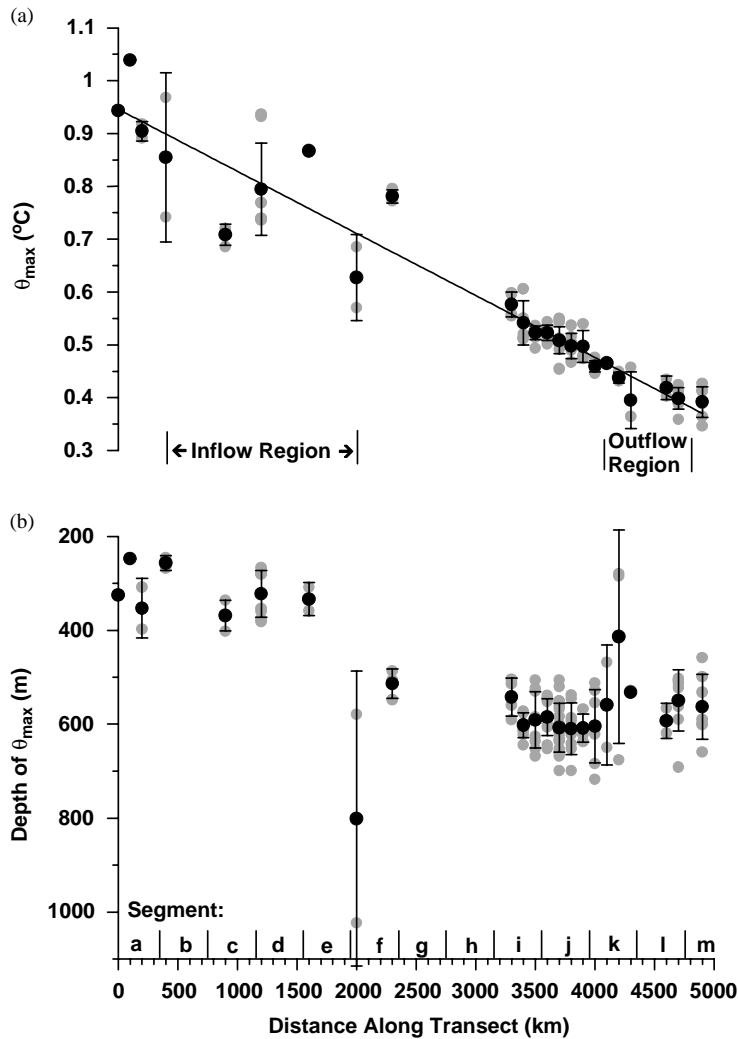


Fig. 3. The average (a) θ_{MAX} (black dots) and (b) depth of θ_{MAX} (black dots) during 1991 to 1995 for each sub-segment along transect B. In (a) and (b) the gray dots show the individual θ_{MAX} and depth of θ_{MAX} values for each of the profiles, respectively. The error bars represent one standard deviation of the values for the respective sub-segment. The solid line in (a) represents a linear fit to the average values. The segments are labeled at the bottom and the locations of the inflow and outflow regions indicated.

working with this data set: significant temporal variability and spatial structure existed on a variety of scales. Some insight into the origins of the temporal variability and spatial structure can be gained from Figs. 4a and 5a. Fig. 4a shows the locations of the profiles from 1990 to 1995 as dots, and Fig. 5a the potential temperature profiles for the different segments. When the data for a segment originated from only one cruise and most

of the profile locations fell along a narrow depth band such as for segments i and j (Fig. 4a), the standard deviations were relatively small (error bars in Fig. 3a). For other segments, such as b and d, the standard deviations were larger and θ_{MAX} values varied up to $\sim 0.2^{\circ}\text{C}$ within the sub-segments (error bars in Fig. 3a). The variability in segment d (Figs. 3a and 5a), where the 5 profile positions were close (less than 10 km apart)

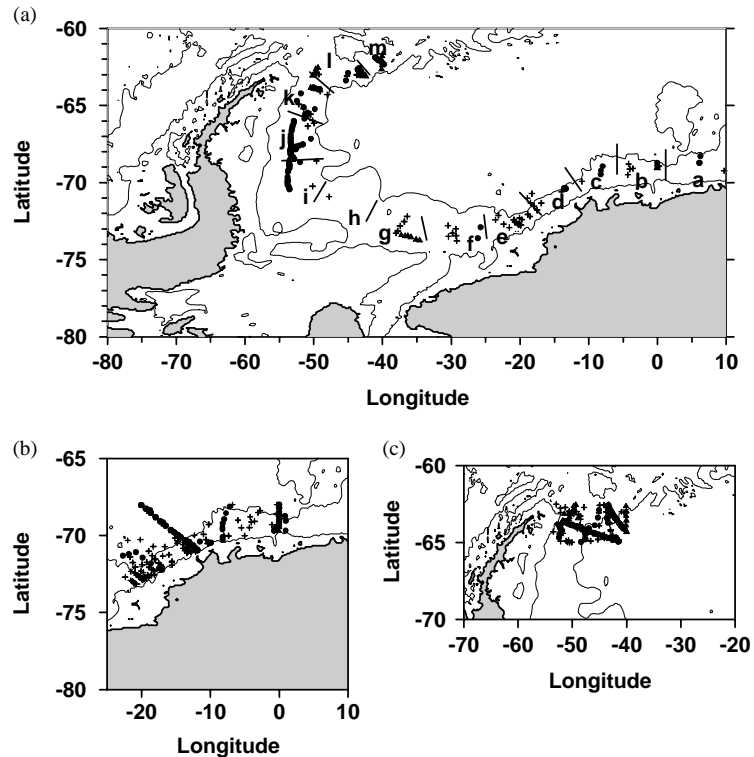


Fig. 4. Locations of CTD or bottle data sites used for all years for (a) transect B, (b) the inflow, and (c) the outflow regions. Depth contours are shown for 500 and 4000 m. The segments are labeled and their extents indicated in (a). Profile locations prior to 1990 are indicated by crosses, those from 1990 to 1995 by dots, and those from 1996 on by triangles.

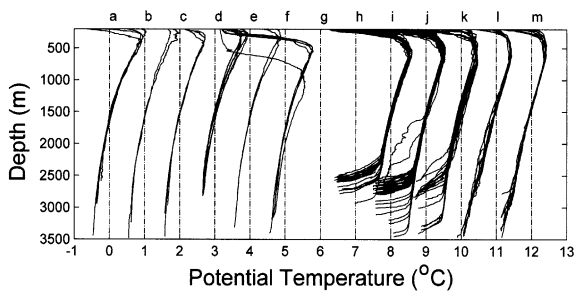


Fig. 5. Profiles of potential temperature, θ , along transect B, for the years 1990–1995, offset by 1°C per segment. Dashed lines indicate the zero line for each set of profiles.

(Fig. 4a), was primarily caused by temporal variability, with θ_{MAX} values from 1993 $\sim 0.2^\circ\text{C}$ warmer than those from 1990 to 1991. Although temporal differences could contribute to the large standard deviations in segment b (profiles from

1992 to 1993), the colder θ_{MAX} value is associated with a different cross-slope position, ~ 30 km south, nearer the continental shelf (Fig. 4a). Other large standard deviations, such as that in the last sub-segment in k, were attributable to different cross-slope positions (Fig. 4a). Additionally, anomalous profiles occurred, such as the one in segment f with an extremely deep and cool θ_{MAX} (Figs. 3a, b, and 5a). Not all of the temporal variability and spatial structure are resolvable on an annual time scale or by the sub-segments. Many local and/or transient processes, such as intrusions, eddies, entrainment of other waters, continental shelf waves, and other processes, induce variability and structure into the profiles, particularly near the continental shelf (Robertson et al., 1995; Gordon et al., 2001). However, resolution or additional discussion of such features falls beyond the scope of this paper.

The θ_{MAX} was located deeper in the water column further along the gyre transect. In the eastern Weddell Sea, the average depth of θ_{MAX} was ~ 330 m; whereas it was ~ 580 m in the western Weddell Sea (Fig. 3b). A distinct increase in the depth of θ_{MAX} occurred around segment f, where the transect passes the Filchner depression, the continental shelf broadens, and Ice Shelf water flows out and enters the Weddell Basin. A thin cold bottom water layer was present downstream from segment f (Fig. 5). Fahrback et al. (1994b) postulated that the deeper θ_{MAX} location is linked to the differences between the two regions for continental shelf widths, offshore locations of the coastal polynyas, and water depths where brine rejection occurs.

In summary, the data set shows significant spatial structure in the maximum temperature strata of the WDW, particularly along the western boundary of the Weddell Gyre. We will take some aspects of this spatial structure into account when analyzing its time variability in the inflow region.

4. Temporal temperature trends

4.1. Warm deep water

To evaluate the temporal trends, the θ profiles in both regions were grouped according to the year and the water depth (Figs. 6 and 7 for the inflow and outflow regions, respectively). The data prior to 1970 were not included as a separate subplot, but were included in the background data set (gray profiles). A pattern emerges with the coldest θ_{MAX} values during the 1970s, warming from the 1970s to the 1990s, and the warmest θ_{MAX} 's during the 1990s in both the inflow and outflow regions (Figs. 6 and 7, respectively), with the exception of one outflow profile in 1988 (Fig. 7c). This profile was cooler by $\sim 0.12^\circ\text{C}$ at θ_{MAX} than three other profiles collected further offshore during the same year. Most of the coldest WDW, as evidenced by the low θ_{MAX} 's, occurred during or just after the Weddell Polynya years (1974–1976) (Figs. 6e, f, 7e and 7f). The profiles prior to 1970 had θ_{MAX} values similar to those of the late 1980s (not shown as a

separate subplot). Furthermore, θ_{MAX} for profiles collected at the same location in segments l and m of transect B consistently differed by $\sim +0.2^\circ\text{C}$ between the early and late 1990s (not shown).

To evaluate further the apparent warming, annual average profiles of θ were determined for the inflow and outflow regions (boxes in Fig. 1a) from 1970 to 2000. The average annual profiles were calculated according to the bottom depths for three depth ranges representing the core of the WDW (3000–3500, 3500–4000, and 4000–4500 m). The θ_{MAX} was determined for each of these average profiles. The potential temperatures of the inflow region were adjusted for distance along the transect using the spatial trend and 12.5°W as a reference point. The average of these θ_{MAX} values for the three depth ranges representing the core are shown in Fig. 8a with the values from the inflow region as black triangles and those from the outflow region as black dots.

The years 1973–1978 and 1984 had the lowest θ_{MAX} values for the inflow and outflow regions (Fig. 8a). One of the two 1984 θ_{MAX} inflow temperatures was $\sim 0.03^\circ\text{C}$ lower due to the presence of a ~ 200 m thick cold intrusion in the WDW. The 1984 outflow profile had no evidence of large intrusions, and there was no apparent reason for the anomalously low value. The other years with low θ_{MAX} values occurred near the time of the Weddell Polynya and their low values are believed to be associated with it. Subsequent to the Weddell Polynya years, warming occurred in both regions, with a general trend of $\sim 0.012 \pm 0.007^\circ\text{C yr}^{-1}$ (dashed lines in Fig. 8a). Although a wide spatial area was used for the inflow region, the temporal trend was robust to this spatial variability, since a similar trend was found without the spatial adjustment.

A shallower WDW layer is more vulnerable to surface mixing processes, such as entrainment of surface waters and erosion, and is more likely to affect the surface ice cover. During the years of the Weddell Polynya, θ_{MAX} was located deeper in the water column, roughly 200 to 300 m, than in the 1980s or 1990s (Figs. 6–8b). The unusually deep locations of θ_{MAX} for 1987 for the inflow region were associated with intrusions. Intrusions contribute to the erosion of the upper WDW and

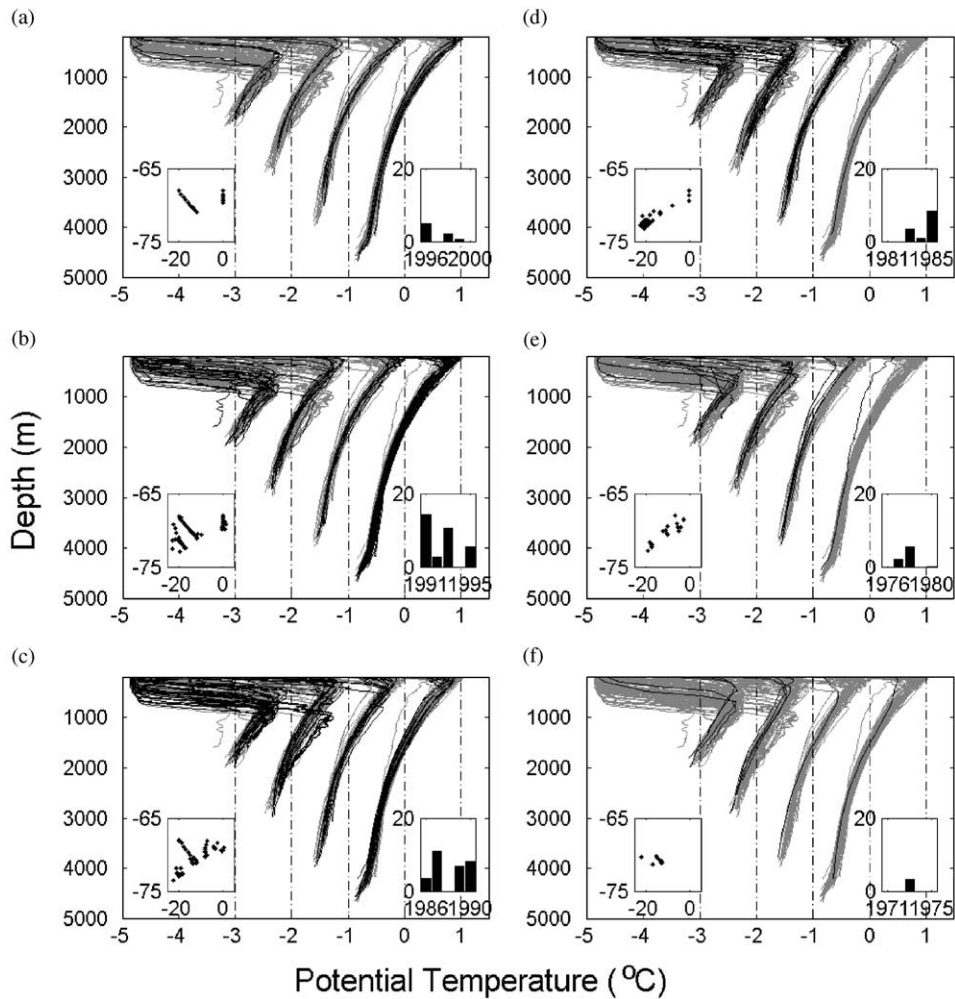


Fig. 6. Profiles of potential temperature, θ , for the inflow region for the depth ranges 1000–2000, 2000–3000, 3000–4000, and 4000–5000 m. The profiles are offset 1°C for each depth range, with the deepest range having no offset. The profiles are highlighted in black for (a) 1996–2000, (b) 1991–1995, (c) 1986–1990, (d) 1981–1985, (e) 1976–1980, and (f) 1971–1975. The pre-1970 data are included in all subplots in gray. Each subplot includes a plot of the CTD and bottle sites and a histogram of the percentage of occurrence of profiles for each year of the subplot. Dashed lines indicate the zero line for each set of profiles. The locations of the profiles are shown in Fig. 4b.

result in a deeper location for θ_{MAX} (Robertson et al., 1995; Gordon, 1998).

How does the temporal warming pattern manifest itself in $\theta - S$ diagrams for the outflow region? Due to calibration errors in some of the data, it was necessary to adjust the salinity in these $\theta - S$ diagrams. For this adjustment, a general $\theta - S$ relationship was determined from the DOVETAIL and CORC cruises for the $\theta - S$

data between 2000 and 3000 m. An average salinity offset for each profile was determined by averaging the difference between the original S values and the S from the $\theta - S$ relationship for the respective θ values. The S values were then adjusted using this average salinity offset, when the offset exceeded 0.01 psu. Most of the adjusted profiles came from two British Antarctic Survey cruises, which had calibration problems (C. Pudsey,

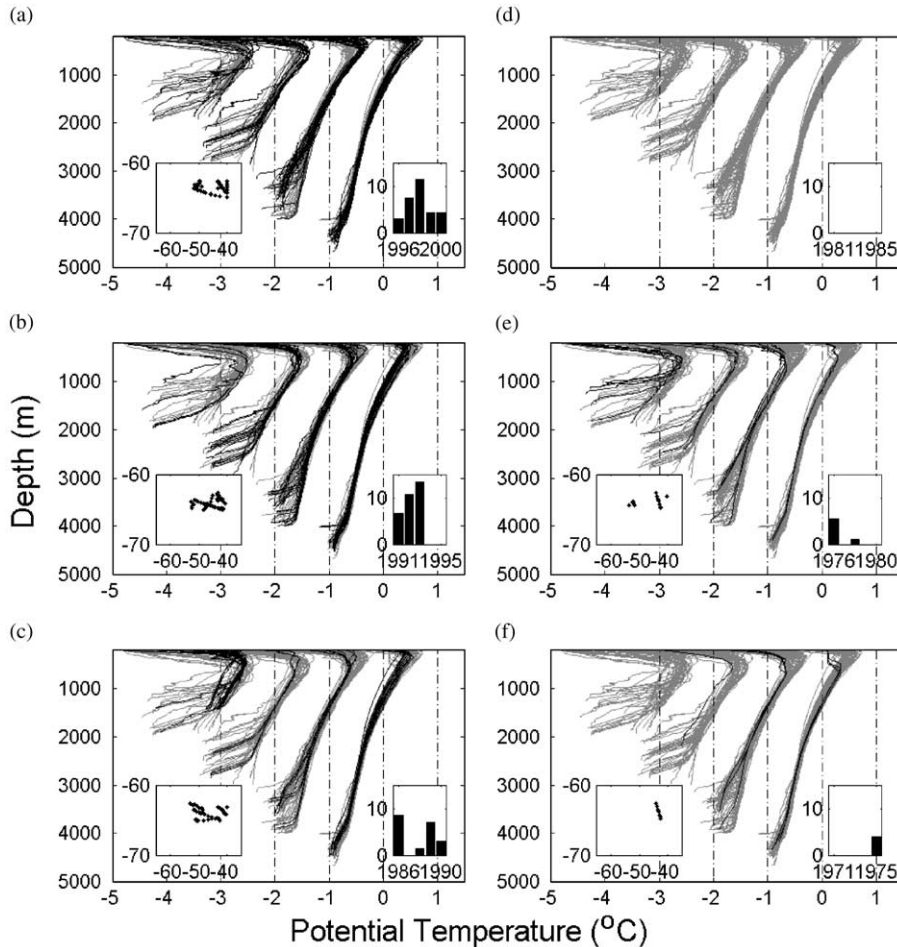


Fig. 7. Profiles of potential temperature, θ , for the outflow inflow region for the depth ranges 1000–2000, 2000–3000, 3000–4000, and 4000–5000 m. The profiles are offset 1°C for each depth range, with the deepest range having no offset. The profiles are highlighted in black for (a) 1996–2000, (b) 1991–1995, (c) 1986–1990, (d) 1981–1985, (e) 1976–1980, and (f) 1971–1975. The pre-1970 data are included in all subplots in gray. Each subplot includes a plot of the CTD and bottle sites and a histogram of the percentage of occurrence of profiles for each year of the subplot. Dashed lines indicate the zero line for each set of profiles. The locations of the profiles are shown in Fig. 4c.

personal communication), and the adjustments were an attempt to address these problems. The spread in the salinity values was attributed to the different calibration techniques used for the different cruises.

It is clear from the $\theta - S$ diagrams that WDW core density changed with time (Fig. 9). The least dense WDW occurred during the late 1990s (Fig. 9a) and the densest WDW during 1976, which is consistent with the time required for deep water from the first Weddell Polynya to transit to

the outflow region (Fig. 9e). This effect was not due to the salinity corrections, since none of the data in Figs. 9a and e were adjusted and it also held when the salinity was not adjusted (not shown).

4.2. Weddell Sea deep water (WSDW)

The temporal behavior of the WSDW was investigated for all profiles in the inflow and outflow regions with water depths greater than

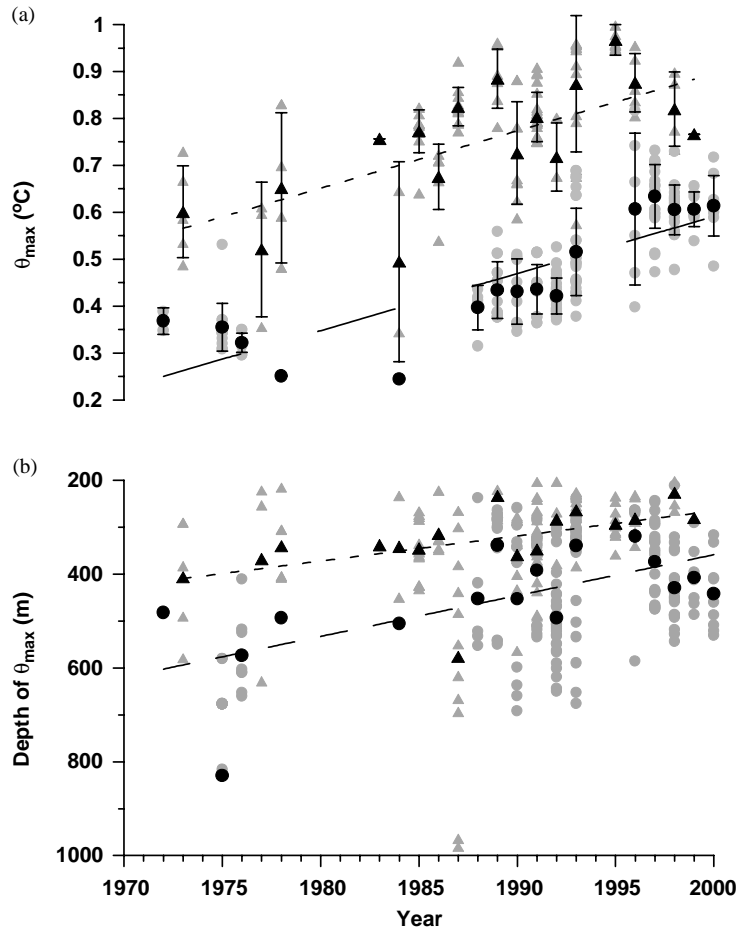


Fig. 8. The average (a) θ_{MAX} and (b) depth of θ_{MAX} over time for the inflow region (black triangles) and the outflow region (black dots) from 3000 to 4500 m water depth. The gray triangles and dots are the values for the individual profiles in the inflow and outflow regions, respectively. The error bars represent one standard deviation of the values. The short and long dashed lines are fitted trends for the inflow and outflow regions, respectively.

4000 m using two 1000-m depth bands from 1500 to 3500 m (Fig. 10). Similar to the WDW, the coldest average WSDW potential temperatures for these depth bands occurred from 1975 to 1977, during or just after the Weddell Polynya (Fig. 10). Although the warmest average potential temperatures occurred during the 1990s, the signal is small and a significant trend could not be determined with the standard deviations. Fahrbach et al. (1998a) used a shorter record (1989–1995) from an array of moorings in the central Weddell Sea and determined a warming trend of $\sim 0.01^{\circ}\text{C yr}^{-1}$ for the WSBW.

5. Discussion

The observed warming trend of $0.012 \pm 0.007^{\circ}\text{C yr}^{-1}$ is comparable to the average warming of the surface of the global ocean since the 1950s, 0.31°C or $\sim 0.007^{\circ}\text{C yr}^{-1}$ (Levitus et al., 2000) and the warming trend of $\sim 0.01^{\circ}\text{C yr}^{-1}$ for the WSBW from 1989–1995 observed by Fahrbach et al. (1998a) in the central Weddell Sea. Although there is no apparent direct connection between the surface ice temperature and the WDW, the trend was also comparable to warming of the surface ice from 1970 to 1998 in the Weddell Sea,

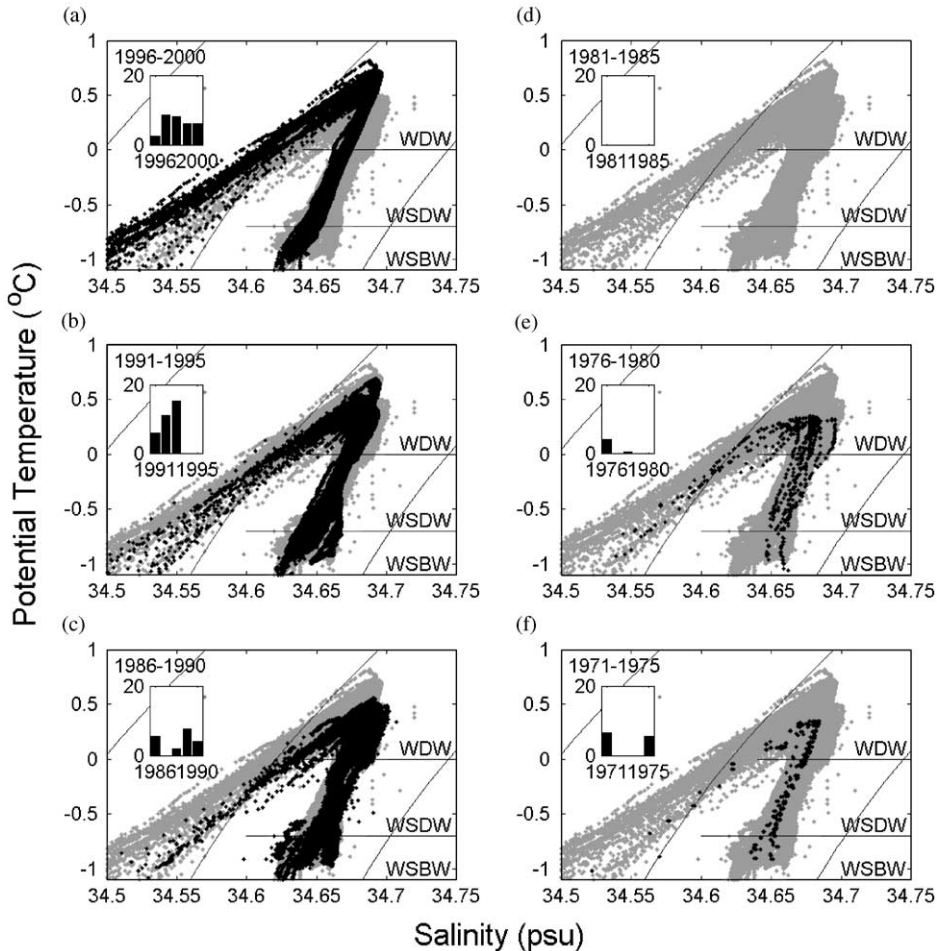


Fig. 9. $\theta - S$ diagrams for the outflow region with the values highlighted in black for (a) 1996–2000, (b) 1991–1995, (c) 1986–1990, (d) 1981–1985, (e) 1976–1980, and (f) 1971–1975. Isopycnal lines are indicated for $\sigma(S, \theta, 0)$. The ranges of the WDW, WSDW, and WSBW are shown. The pre-1970 data are included in all subplots in gray. Each subplot includes a histogram of the percentage of occurrence of profiles for each year of the subplot.

$\sim 0.01\text{--}0.02^\circ\text{Cyr}^{-1}$, observed in satellite data by Comiso (2000).

We evaluated the trends over the time period after the Weddell Polynya closed. Events such as the Weddell Polynya, 1974–1976, lowered the WDW and WSDW potential temperatures by a few tenths of a degree and were associated with most of the lowest values in our record (Figs. 6–8). This agrees with the observed average and a maximum cooling in the deep basin during the Weddell Polynya of 0.2°C and 0.4°C , respectively, reported by Gordon (1982). Cool WDW

occurred in 1973 and may indicate either that the path of the circulation was altered and the warm circumpolar deep water flowing into the region missed our locations or cooler circumpolar deep water entered the region at this time. After the Weddell Polynya, a warming trend existed with temperatures during the late 1980s equivalent to those prior to the Weddell Polynya and the warmest temperatures occurring during the late 1990s (Fig. 8a). This indicated not only a return to conditions prior to the polynya, but subsequent further warming. The warming trend

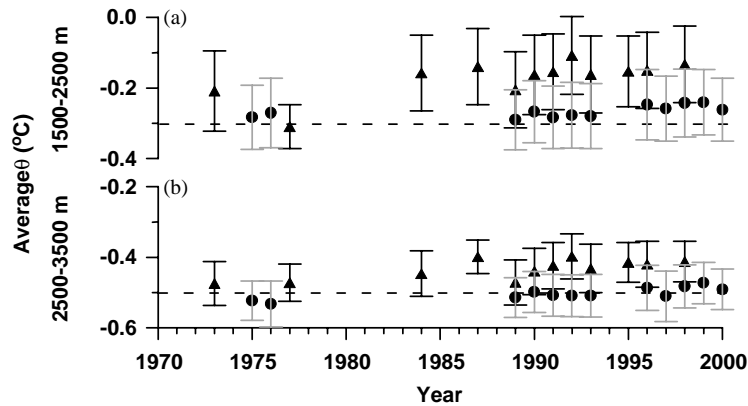


Fig. 10. The average potential temperature, θ , for the inflow (triangles) and outflow (dots) regions for the depth ranges (a) 1500–2500 m and (b) 2500–3500 m over time. The error bars represents one standard deviation of the values. Dashed reference lines indicate -0.3°C and -0.5°C in (a) and (b), respectively.

was not uniform and had fluctuations superimposed on it (Fig. 8a).

There are two basic mechanisms by which warming of the upper layers can occur; increased inflow of warmer water, or changes in the cooling processes within the Weddell Sea. If warming is due only to the inflow of warmer water or the increased inflow of warm water, both the inflow and outflow waters should change with a ~ 2 –4-year lag for transit around the gyre. Differences due to changes in the cooling processes occurring within the gyre should affect the outflow waters more than the inflow waters. For example, if the velocity of the gyre increases due to increased wind stress, the transit time around the gyre is reduced. If the mixing processes remain the same, the cooling during transit will also be reduced. The result will be an apparent warming of the outflow waters relative to the inflow waters, although increased wind stress also could modify the inflow waters. As a rough estimate, an increase (reduction) in gyre velocity of 20% will increase (reduce) the outflow θ_{MAX} by $\sim 0.07^\circ\text{C}$. As another example, cooling by a large polynya should affect the outflow waters much more than the inflow waters, although the conditions for development of a large polynya might be linked to changes in the inflow waters.

Since equivalent temporal trends occurred in the inflow and outflow regions (Fig. 8a), the primary

cause of warming is, based on the above, probably due to a change in the inflow waters rather than a change in the cooling processes within the Weddell Basin. There appears to have been less inflow of circumpolar deep water or a cooler version of circumpolar deep water during the early 1970s and inflow of warmer or a higher volume of circumpolar deep water in the 1990s, particularly the late 1990s. Because of the large number of data gaps in Fig. 8a, we cannot preclude that processes within the Weddell Gyre also play a role. In fact, the processes should both dampen some fluctuations and induce others dependent on the occurrence of their forcing processes, particularly for the outflow region. For example, Nøst and Østerhus (1995) have suggested that the grounding of several large icebergs in 1987–1988 decreased Ice Shelf water and WSDW production and resulted in higher salinity of WSDW.

An increase in inflow temperature or amount would occur if the Weddell Front moved south increasing the inflow of circumpolar deep water into the Weddell Gyre. The cooling in the late 1990s may be related to movement of the Weddell Front. Both the Antarctic Oscillation /Southern Annular Model (SAM) and the Antarctic circumpolar wave (ACW) are capable of shifting the position of the Weddell Front. The Antarctic oscillation/SAM is an annular mode similar to the Arctic oscillation, where the atmospheric pressure

conditions fluctuate between positive and negative indices (Thompson and Wallace, 2000). It occurs at irregular intervals with a strong trend in the recent years (Dickson et al., 2001). Its influence on the Weddell Sea Gyre water mass properties and circulation are not well known and are subject to further research. Another independent phenomenon, the ACW, is a slowly moving wave characterized by sea-surface height and temperature anomaly, which propagates eastward around Antarctica (White and Peterson, 1996; Jacobs and Mitchell, 1996). The ACW has been observed to modify the position of the southern front of the ACC and the surface ice extent. It has a dominant 4- or 6-year period (White and Peterson, 1996; Jacobs and Mitchell, 1996). Gaps in the data prevented definitive identification of the correlation between either the SAM or the ACW and the temperature fluctuations (Fig. 8a).

Although some useful statements about the warming trend of the WDW could be made, the expected weaker signal of the WSDW, particularly the high temporal variability of the WSDW properties, precluded similar assessments. Thus, there is a pressing need to establish and maintain a reference data set in the Weddell Sea Gyre. A start in this direction has been made as part of the southern component of the CORC program and by the Alfred-Wegener-Institut. In the CORC program, it is planned to collect annual time series of CTD and mooring data over a period of 10 years for a transect in the outflow region. This program is presently in its third year and will provide a more extensive data set for the outflow region for 1999–2009.

Acknowledgements

We are grateful to G. Rohardt, K. Nicholls, and C. Pudsey for providing us with data for this work. Additionally, B. Huber and P. Mele helped assemble the data available at LDEO. We would also like to thank three anonymous reviewers for their constructive comments, which greatly improved the manuscript. This study was funded by grant UCSIOPO 10075411 from the National Oceanic and Atmospheric Agency (NOAA). The

views expressed herein are those of the authors and do not necessarily reflect the views of NOAA or any of its subagencies. This is Lamont publication 6356.

References

- Barber, M., Crane, D., 1995. Current flow in the northwest Weddell Sea. *Antarctic Science* 7, 39–50.
- Carmack, E.C., Foster, T., 1977. Water masses and circulation in the Weddell Sea. In: *Polar Oceans, Proceedings of the Polar Oceans Conference, Montreal, 1974*. Arctic Institute of North America, Calgary, Canada, pp. 151–165.
- Comiso, J.C., 2000. Variability and trends in Antarctic surface temperatures from in situ and satellite infrared measurements. *Journal of Climate* 13, 1674–1696.
- Conkright, M.E., Levitus, S., O'Brien, T., Boyer, T.P., Antonov, J.I., Stephens, C., 1998. *World Ocean Atlas 1998 CD-ROM Data Set Documentation*. NODC Internal Report 15, Silver Springs, MD, 16pp.
- Deacon, G.E.R., 1937. The hydrology of the Southern Ocean. *Discovery Reports* 15, 1–124.
- Deacon, G.E.R., 1979. The Weddell gyre. *Deep-Sea Research* 26A, 981–995.
- Dickson, R.R., Hurrell, J.W., Bindoff, N.L., Wong, A.P.S., Arbic, B., Owens, B., Imawaki, S., Yashayaev, I., 2001. The world during WOCE. In: Siedler, G., Church, J. (Eds.), *Ocean Circulation and Climate, WOCE IPO, 77*, International Geophysics Series. Academic Press, New York, pp. 557–583.
- Fahrbach, E., Rohardt, G., Schröder, M., Strass, V., 1994a. Transport and structure of the Weddell Gyre. *Deep-Sea Research* I 41, 389–411.
- Fahrbach, E., Peterson, R.G., Rohardt, G., Schlosser, P., Bayer, R., 1994b. Suppression of bottom water formation in the southeastern Weddell Sea. *Annales de Geophysicae* 12, 840–855.
- Fahrbach, E., Meyer, R., Rohardt, G., Schröder, M., Woodgate, R.A., 1998a. Gradual warming of the Weddell Sea deep and bottom water. *Filchner–Ronne Ice Shelf Program, Report No. 12*, Alfred-Wegener-Institut, Bremerhaven, Germany, pp. 24–34.
- Fahrbach, E., Schröder, M., Klepikov, A., 1998b. Circulation and water masses in the Weddell Sea. In: Leppäranta, M. (Ed.), *Physics of Ice-Covered Seas, Vol. 2*. Helsinki University Press, Helsinki, pp. 569–603.
- Fahrbach, E., Harms, S., Rohardt, G., Schröder, M., Woodgate, R.A., 2001. Flow of bottom water in the northwest Weddell Sea. *Journal of Geophysical Research* 106, 2761–2778.
- Fofonoff, N.P., Millard, R.C., 1983. Algorithms for computation of fundamental properties of seawater, UNESCO Technical Report on Marine Sciences, 44.
- Gordon, A.L., 1982. Weddell deep water variability. *Journal of Marine Research* 40, 199–217.

- Gordon, A.L., 1998. Western Weddell Sea thermohaline stratification, ocean, ice, and atmosphere: interactions at the Antarctic continental margin. *Antarctic Research Series* 75, 215–240.
- Gordon, A.L., Huber, B.L., 1990. Southern Ocean winter mixed layer. *Journal of Geophysical Research* 95, 11655–11672.
- Gordon, A.L., Huber, B.L., 1995. Warm Weddell deep water west of Maud Rise. *Journal of Geophysical Research* 100, 13747–13753.
- Gordon, A.L., Visbeck, M., Huber, B., 2001. Export of Weddell Sea deep and bottom water. *Journal of Geophysical Research* 106, 9005–9017.
- Gouretski, V.V., Danilov, A.I., 1993. Weddell Gyre: structure of the eastern boundary. *Deep-Sea Research I* 40, 561–582.
- Jacobs, G.A., Mitchell, J.L., 1996. Ocean circulation variations associated with the Antarctic circumpolar wave. *Geophysical Research Letters* 23, 2947–2950.
- Levitus, S., Antonov, J.I., Boyer, T.B., Stephens, C., 2000. Warming of the World Ocean. *Science* 287, 2225–2229.
- Locarnini, R.A., Whitworth III, T., Nowlin Jr., W.D., 1993. The importance of the Scotia Sea on the outflow of Weddell Sea deep water. *Journal of Marine Research* 51, 135–153.
- McPhee, M., Martinson, D.G., 1994. Turbulent mixing under drifting pack ice in the Weddell Sea. *Science* 263, 219–220.
- McPhee, M.G., Ackley, S.F., Guest, P., Huber, B.A., Martinson, D.G., Morison, J.H., Muench, R.D., Padman, L., Stanton, T.P., 1996. The Antarctic flux zone experiment. *Bulletin of the American Meteorological Society* 77, 1221–1232.
- Meredith, M.P., Locarnini, R.A., Van Scoy, K.A., Watson, A.J., Heywood, K.J., King, B.A., 2000. On the sources of Weddell Gyre Antarctic bottom water. *Journal of Geophysical Research* 105, 1093–1104.
- Muench, R.D., Hellmer, H.H., 2002. The International DOVE-TAIL Program: an overview. *Deep-Sea Research II* 49 (21), 4711–4714.
- Muench, R.D., Padman, L., Howard, S.L., Fahrback, E., 2002. Upper ocean diapycnal mixing in the northwestern Weddell Sea. *Deep-Sea Research II* 49 (21), 4843–4861.
- Nicholls, K., Padman, L., Jenkins, A., 1998. First physical oceanography results from the ROPEX98 cruise in the southern Weddell Sea. Filchner–Ronne Ice Shelf Program, Report No. 12, Alfred-Wegener-Institut, Bremerhaven, Germany, pp. 51–58.
- Nøst, O.A., Østerhus, S., 1995. Impact of grounded icebergs on the hydrographic conditions near the Filchner Ice Shelf, Antarctica. *Journal of Geophysical Research*, submitted for publication.
- Orsi, A.H., Nowlin Jr., W.D., Whitworth III, T., 1993. On the circulation and stratification of the Weddell Gyre. *Deep-Sea Research* 40, 169–203.
- Orsi, A.H., Johnson, G.C., Bullister, I.L., 1999. Circulation, mixing, and production of Antarctic bottom water. *Progress in Oceanography* 43, 55–109.
- Robertson, R., Padman, L., Levine, M.D., 1995. Fine structure, microstructure, and vertical mixing processes in the upper ocean in the western Weddell Sea. *Journal of Geophysical Research* 100, 18517–18535.
- Schröder, M., Fahrback, E., 1999. On the structure and the transport of the eastern Weddell Gyre. *Deep-Sea Research II* 46, 501–527.
- Thompson, D.W.J., Wallace, J.M., 2000. Annular modes in the extratropical circulation. Part I: month-to-month variability. *Journal of Climate* 13, 1000–1016.
- Visbeck, M., Gordon, A., Smethie, B., Schlosser, P., Toole, J., Huber, B., Krahnemann, G., 2001. The CORC/ARCHES observing system for Weddell Sea deep and bottom water variability. *Clivar Exchanges* 6, 23–26.
- Weppernig, R., Schlosser, P., Khatiwala, S., Fairbanks, R.G., 1996. Isotope data from Ice Station Weddell: implications for deep water formation in the Weddell Sea. *Journal of Geophysical Research* 101, 25,723–25,739.
- White, W.B., Peterson, R.G., 1996. An Antarctic circumpolar wave in surface pressure, wind, temperature, and sea ice extent. *Nature* 380, 699–702.
- Whitworth III, T., Nowlin, W.D., Locarnini, R.A., Smith, S.G., 1994. Weddell Sea shelf water in the Bransfield Strait and Weddell–Scotia Confluence. *Deep-Sea Research I* 41, 629–641.
- Woodgate, R.A., Schröder, M., Østerhus, S., 1998. Moorings from the Filchner Trough and the Ronne Ice Shelf front: preliminary results. Filchner–Ronne Ice Shelf Program, Report No. 12, Alfred-Wegener-Institut, Bremerhaven, Germany, pp. 85–90.